ISSN 1990-7931, Russian Journal of Physical Chemistry B, 2018, Vol. 12, No. 8, pp. 1205–1211. © Pleiades Publishing, Ltd., 2018.
Original Russian Text © Yu.D. Ivakin, M.N. Danchevskaya, 2018, published in Sverkhkriticheskie Flyuidy. Teoriya i Praktika, 2018, Vol. 13, No. 1, pp. 4–15.

Analysis of Recrystallization of Fine-Crystalline Corundum in a Supercritical Water Medium Using the Lognormal Particle Size Distribution Function

Yu. D. Ivakin[a], * and M. N. Danchevskaya[a]

[a] *Faculty of Chemistry, Moscow State University, Moscow, 119991 Russia*

**e-mail: Ivakin@kge.msu.ru*

Received February 16, 2017

Abstract—The mechanism of synthesis of fine-crystalline corundum from aluminum hydroxide under induced nucleation conditions in a supercritical water fluid at 400°C and initial pressure of 26.4 MPa followed by exposure in the synthesis medium was studied. The crystal size distribution was analyzed by electron microscopy. The use of the lognormal function to describe the crystal size distribution of the synthesized corundum particles was substantiated. The possibility of using the lognormal particle size distribution function and the time dependence of its parameters to reveal the routes of product formation was analyzed. The dimensional spectrum of microcrystals has four components, whose appearance is associated with different routes of product formation. The number of distribution components remains unchanged during prolonged exposure, but their average characteristics have different time dependences. The mass redistribution during recrystallization, generally leading to a decrease in the average crystal size, is explained by differences in the crystal structure mobility of different components. It was concluded that the states of corundum in the newly formed crystals and in the overgrown layer on the particles of the inducing additive are different.

Keywords: fine-crystalline corundum, sub- and supercritical water, solid phase mobility, crystal formation, microcrystal size distribution, lognormal function, coalescence, surface spreading, recrystallization

DOI: 10.1134/S1990793118080055

INTRODUCTION

When γ-$Al(OH)_3$ (aluminum hydroxide, hydrargillite) is treated in a supercritical water fluid (400°C, 26.8 MPa), the formation of fine-crystalline α-Al_2O_3 (corundum) is promoted by adding a small amount of electrocorundum [1]. Spontaneous corundum nucleation is hindered, while the introduction of crystalline corundum particles causes induced nucleation and accelerated transformation in the reaction space. Under the treatment conditions, alumina and its hydrated forms do not dissolve in the water fluid, and the process occurs by the solid-phase mechanism. The size distribution of the formed microcrystals was studied by analyzing the images obtained with a scanning electron microscope (SEM images). For this purpose, the elementary components were sought by deconvolution in the constructed experimental particle size distribution in a way similar to the decomposition of a complex spectrum into the bands of several centers [2–7]. In this case, the logarithmically normal (lognormal) distribution was used for describing the set of forming crystals.

The lognormal distribution differs from the normal one in the use of the logarithm of the random value instead of the latter in the equation for the distribution density [8, 9]:

$$y = \frac{A}{\sigma\sqrt{2\pi}} \exp\left[-\frac{(x-\mu)^2}{2\sigma^2}\right],$$

for the normal distribution, and

$$y = \frac{A}{wx\sqrt{2\pi}} \exp\left[-\frac{(\ln x - \ln m)^2}{2w^2}\right], \quad (1)$$

for the lognormal one.

Here, x is a random variable (particle diameter in this case); A is the coefficient that is proportional to the number of particles; σ is the standard deviation of x; w is the standard deviation of $\ln x$; μ, m is the average value (distribution median).

The normal and lognormal distributions are used to describe a large number of various phenomena [10–13], but they have different applications. The normal distribution is widely used in spectroscopy, for example, in the above-mentioned deconvolution of light emission and absorption spectra [2–7]. At the normal distribution of the random variable, the action of independent factors is the sum of effects and reflects the

additive properties of the system [10, 11]. In this case, the arbitrary system is the sum of individual events (electron transition, measurement error, deviation during the shooting), which is affected by one of the group of incompatible effects. The imcompatibility of effects here is due to the difference in their nature [10]. For example, in the light emission or absorption acts, the electron transition energy is affected by the inhomogeneity of the local environment, temperature, electron-phonon interaction, or electric and magnetic fields. According to the probability theory, the probabilities of incompatible effects are summed [14].

The lognormal function started to be used for particle size analysis in the 1920s [15]. Using the statistical approach, A.N. Kolmogorov derived the lognormal size distribution for particles formed during the grinding [16]. R.B. Bergman and coauthors [17–19] gave an analytical derivation of the lognormal size distribution during crystallization based on the concepts about random nucleation and different growth mechanisms of particles. Selection of the theoretical law of size distribution of the structure elements of metal materials showed agreement with the lognormal distribution with the use of chi-squared Pearson and Kolmogorov–Smirnov tests [20]. The disperse state of the drops of the atmospheric mist formed during vapor condensation has a lognormal distribution [15, 21].

The lognormal distribution describes a random variable, whose variation under the action of many independent factors is proportional to the value already reached at that moment of time. Thus, because of the wear-out of devices or crystal grinding, the mechanical impulses lead to defects, and the next impulses affect the system with already accumulated defects. The effects caused by the action of various factors on the random variable accumulate in the system and add up, with their probabilities being multiplied according to the theory [14]. The system is called multiplicative due to this property [10, 13, 22]. When fine-crystalline powder forms, the random variable (crystal size) is affected by many independent factors such nucleation, coalescence of neighboring particles, and build-up of the mass of the forming crystal due to the appearance of new portions of product substance in the system. The change in the random variable under the action of every next factor is proportional to the value of the quantity already reached by the given moment of time; i.e., the action is multiplicative [22], and the size of the resulting crystals should be described by the lognormal function. The lognormal distribution can reflect the existence of several components that refer to physically different processes [11, 23, 24]. That is, the composition of the sample (multicomponent character) and the corresponding multimodality of distribution (several components with diverse parameters), both normal and lognormal, is related to the contribution of different processes to the formation of the random variable [24, 25].

In the present study, we analyzed the possibility of using the lognormal particle size distribution function and the time dependence of its parameters for determining the formation routes of product crystals using induced synthesis of corundum powder as an example.

EXPERIMENTAL

In the present work, we studied the change in the particle size composition of fine-crystalline corundum in the course of prolonged treatment under the synthesis conditions. Fine-crystalline corundum was synthesized by treatment of a mixture of powders of finely disperse hydrargillite (aluminum hydroxide) and electrocorundum M5 at 400°C and initial pressure of supercritical fluid of 26.4 MPa. The average size of finely disperse hydrargillite particles (Pikalev Alumina Refinery) was 3.46 ± 0.06 μm. The particles of the industrial white electrocorundum M5 powder had a close size, 2.82 ± 0.02 μm [1]. A mixture of components was sieved five times through a capron mesh (mesh size 300 μm) for homogeneous distribution of powder particles. Stainless steel containers with a dry mixture of hydrargillite (2 g) and M5 powder (1 mg) prepared by the same procedure were placed in three autoclaves with a volume of ~19 cm^3. The reaction mixture was loosely poured into the containers. The content of the M5 additive was 0.05 wt % of the amount of hydrargillite or 0.076 wt % of the mass of the resulting corundum. Distilled water was poured on the bottom of the autoclave outside the container, which was mounted on a support above the water level. The amount of water was such that 20% of the empty space of the autoclave was filled together with the water isolated from hydrargillite at the stage of formation of boehmite by the reaction

$$Al(OH)_3\,(2\,g) \rightarrow AlOOH\,(1.538\,g) + H_2O\,(0.462\,g).$$

When the autoclave is heated to 400°C, hydrargillite transforms into boehmite, whose dehydroxylation under the isothermal conditions of heating forms corundum [1, 26]. The calculated pressure of the supercritical water fluid (SCWF) heated to 400°C is 26.4 MPa [27]. It increases to 26.7 MPa due to the isolation of water during dehydroxylation of boehmite. Then the pressure does not change after the storage of the resulting corundum under the isothermal conditions. The autoclaves were kept at 400°C: one for 21 h (this corresponds to 100% formation of corundum [1]), the other for 45 h, and the third for 73 h. After the keeping at 400°C was completed, the bottom of the autoclave was submerged in water. The water vapor condensed on the bottom, and the resulting corundum remained dry in the container.

The morphology and size distribution of crystals in the samples were determined by analyzing the SEM images (JSM-6390LA SEM microscope). Several micrographs for different sites of the sample were used. For isometric particles, the characteristic of

their size is the diameter. For elongated or irregular particles, the area of the image contour of the particle was measured. In this case, the average equivalent diameter of the particle $d_{eq} \pm \Delta d$, where $\Delta d = d_{eq}(\Delta S/2S)$ is calculated from the average area of the particle contour $S \pm \Delta S$ using the formula $d = (4S/\pi)^{1/2}$.

As a result of measurements, two types of the average sizes were found. The general average size D (μm) is determined by simply averaging the sizes of all particles.

The second type of the average size is determined by the following procedure. A distribution histogram is constructed based on the results of measurements of particle diameters in the form of the dependence of the number of particles (frequency) that appear in the grouping interval (the region of uniform distribution of the whole range of the observed particle sizes) on the position of the interval on the crystal size axis. Then the dependence of the number of particles in the grouping interval on the size in the middle of the interval is constructed, which transforms, after division by the total number of calculated particles, into the dependence of the mean probability density (relative frequency) on the particle size.

Then the number and characteristics of the continuous functions are determined by computer deconvolution, the sum of the functions being optimum for describing the dependence of the mean probability density on the particle size. If the experimental distribution is described by one or more lognormal functions (Eq. (1)), each function is characterized by the coefficient A (the area under the distribution curve) and the parameters m (average size (distribution median)) and w (distribution width, which characterizes the form of the distribution function). In the constructed total continuous polymodal distribution, each component or individual function with its parameters describe the individual component of complex composition formed by different physical processes. The error of the calculated distribution parameter corresponds to 95% confidence probability.

The physical meaning of the w parameter responsible for the distribution width can easily be understood if we imagine that the crystals form under identical conditions and have identical sizes. In this case, the distribution function has a narrow width and a symmetrical contour of the dependence of the probability density on the crystal size. An increase in the distribution width means an increase in the differences under the crystal formation conditions. The distribution function becomes asymmetric (skewed), with an elongated right wing. The higher the w value and, accordingly, the higher the asymmetry of the distribution, the greater the deviation (shift to the left) of the maximum on the size distribution density curve versus $x = m$.

As to the m value, it is obtained (more exactly, its logarithm) by averaging the logarithms of the particles size; i.e.,

$$\ln m = (1/N)\sum_i (n_i \ln d_i)$$

or

$$m = \left[\prod_i (d_i)^{n_i}\right]^{(1/N)}, \quad (2)$$

where N is the total number of measured particles, and n_i is the number of particles with the same d_i.

Equation (2) shows that in contrast to the average diameter D, which can be determined as a mean arithmetic, the m parameter is the mean geometrical value of the particle size of the component.

The efficiency of deconvolution depends on the choice of the step of partitioning into grouping intervals. The choice is dictated by two boundaries. If the width is excessive, the details of the distribution can be lost. Step minimization leads to a scatter of points because of an error in determining the average distribution density in the grouping interval and the small number of particles in it. For satisfactory description of the distribution by one lognormal function (so-called unimodal case corresponding to disperse powder with one component), it suffices to calculate the sizes of ~1000 particles. If the scatter of points did not allow stable deconvolution, additional SEM micrographs of the sample were processed to increase the number of calculated particles and improve the statistics in the grouping interval. In the case of several modules, the number of particles was occasionally increased to 3000–9000 (6–12 micrographs). If the number of components of the distribution was not expressed in explicit form, an additional (e.g., second) module was introduced when some experimental points departed from the approximating function on an extensive region of particle size (generally in the tail of the distribution). For random position of the experimental points near the total function, it was assumed that addition of a new module is physically senseless.

RESULTS

Figure 1 shows the SEM images of the synthesized samples and the result of approximation of the experimental points (solid line) of the crystal size distribution. The crystals are isometric; the largest diagonal of the image contour was taken as a size. The figures clearly show the signs of the four components of the size distribution. The contours of the components revealed by deconvolution are shown by the dashed lines. The parameters of the distribution functions of the crystals of different components are summarized in Table 1. The transformation of boehmite into corundum is related to the induced seed formation and crystal growth due to the surface spreading of nuclei [1]. The difference in the crystal growth in different regions of the reaction space leads to the appearance of the distribution components. After 21-h treatment of boehmite, the formation of corundum is completed, and

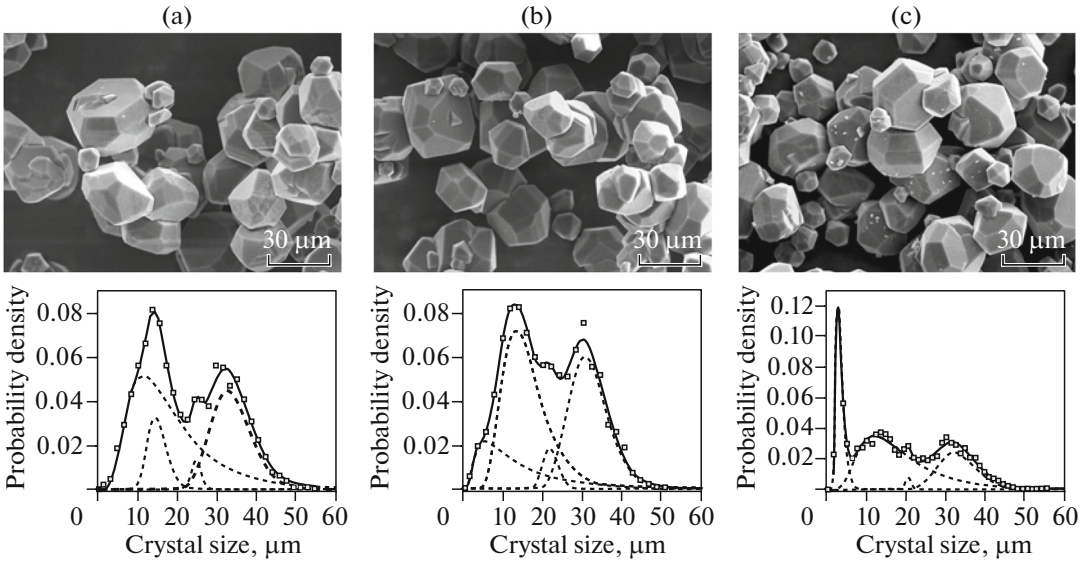

Fig. 1. SEM images and crystal size distribution for corundum samples after exposure in the synthesis medium for (a) 21, (b) 45, and (c) 73 h.

the change of the parameters of the distribution functions of the components with time indicates that the slowest process (redistribution of mass between crystals with different structure mobilities) continues. The recrystallization is evidently related to the diffusion spreading of the substance of the crystals possessing a mobile structure over the surface of the crystals with lower structure mobility until the counter flows of the mass become equal. The crystals with increased structure mobility lose the mass and are diminished. The total range of crystal size from 0 to ~55 μm remains unchanged during the treatment. The overall average crystal size of corundum decreases during the treatment time (Fig. 2). The average crystal size of the four components changes differently (Table 1), decreasing for the first and third components, increasing for the second component, and changing little for the fourth one. Consequently, the crystals of the components differ in the structure mobility. The crystals belong to different components depending on the average size and distribution width. When the mass is redistributed, both parameters change, and the assignment of crystals to components also changes. Interestingly, the number of components remains the same when the treatment time increases. The fourth component is least liable to changes.

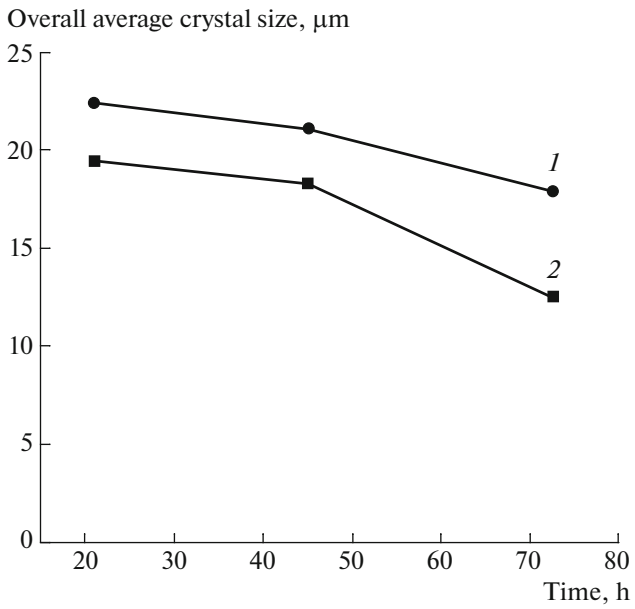

Fig. 2. Dependence of the overall average crystal size on the treatment time: (*1*) arithmetic averaging and (*2*) geometrical averaging.

The first, second, and third components of the distribution characterize the newly formed crystals. The forth component of the distribution with the highest average crystal size (m_4) belongs to the crystals from the grown particles of the M5 additive [1]. The same w_4 value for the three samples (0.153 ± 0.012, 0.158 ± 0.015, 0.15 ± 0.01; Table 1) suggests that the conditions of additive grain build-up were identical and did not change when the mass was redistributed. The number of crystals of this component corresponds to the same number of additive particles in the reaction mixture. In Table 1, the A_i values that are proportional to the number of crystals are given in two columns. In the right column they are normalized to A_4 and show the number of new crystals per additive grain; in the left column, they were recalculated into the fractions of components α_i provided that $\Sigma\alpha_i = 1$.

Table 1. Parameters of the components of crystal size distribution at different storage times under the synthesis conditions

Parameter	Time, h					
	21		45		73	
A_1*	0.555	1.77	0.167	0.48	0.219	0.93
A_2*	0.110	0.35	0.441	1.26	0.534	2.26
A_3*	0.022	0.07	0.042	0.12	0.011	0.05
A_4*	0.313	1	0.350	1	0.236	1
m_1**	15.8 ± 1.1		10.8 ± 8.7		2.50 ± 0.05	
m_2**	14.65 ± 0.30		14.7 ± 0.7		15.7 ± 0.8	
m_3**	24.7 ± 0.5		21.6 ± 0.7		20.1 ± 0.4	
m_4**	33.4 ± 0.3		31.1 ± 0.3		32.50 ± 0.25	
w_1	0.587 ± 0.037		0.90 ± 0.25		0.38 ± 0.01	
w_2	0.169 ± 0.029		0.37 ± 0.05		0.55 ± 0.04	
w_3	0.049 ± 0.019		0.088 ± 0.035		0.04 ± 0.02	
w_4	0.153 ± 0.012		0.158 ± 0.015		0.15 ± 0.01	

* The A_i values in the left column were recalculated to $\Sigma A_i = 1$, and those in the right column were normalized to A_4.
** The values are given in μm.

When the mass is redistributed, the total amount of corundum evidently does not change and equals the sum of the masses of the components.

DISCUSSION

In the reaction space limited by the bulk volume of the starting mixture, the distance between the uniformly distributed additive grains is 56.2 μm (Eq. (3) in [1]). The space between the additive grains is filled with small boehmite crystals 0.5–1.0 μm in size. The build-up of additive particles (grains) occurs from the surrounding spherical zone, which has a diameter of 37.8 μm according to the data of [1]. Consequently, the spherical zones of additive grain build-up are separated by a distance of 56.2 – 37.8 = 18.4 μm. Thus, the space consists of two parts. One part are the additive grain build-up zones, and the other part lies in the space between them. According to the concepts put forward in [1, 26], the corundum nuclei form during the dehydroxylation of boehmite at the same probability in the whole space. Further crystal formation, however, depends on the environment. In the zone around the additive grains, some part of the forming alumina in the form of corundum nuclei with a disordered structure diffuses to the additive particles and forms the crystals of the fourth component of the crystal size distribution of the product of transformation. The rest of corundum seeds form the crystals of the third component of the distribution. By the moment when boehmite completely transforms into corundum (21 h of treatment), the conditions of crystal formation of the third component are most uniform because w_3 has the minimum value (Table 1). The crystals of the first and second components form in the space between the additive grain build-up zones. A build-up zone appears around the first crystals of the second component, in which the crystals of the first component form from the remaining nuclei. The conditions of crystal build-up of the second component are close to those of the additive grains because the w_2 and w_4 values differ insignificantly (Table 1). The crystals of the first component form under various conditions of space that remained between the additive grain build-up zones and the crystals buildup zones of the second component. Thus, the crystals of the fourth component appear due to the collective build-up of additive grains, and the crystals of the first, second, and third components form as a result of free generation. The distribution width w_1 is maximum (Table 1, 21-h treatment). The structure of the crystals of the first component is evidently most disordered and hence most mobile. After boehmite was exhausted and nucleation stopped, the build-up of the crystals of the second component continues due to the surface spreading of the spatially close disordered crystals of the first component. Some crystals of the first component are united; i.e., they coalesce due to the spreading over the larger crystals. The thus formed crystals behave like crystals of the second and third components because the fraction of these components increases after 45-h treatment (left column, Table 1, $\alpha_2 = 0.441$ and $\alpha_3 = 0.042$), and the fraction of the crystals of the first component decreases from 0.555 to 0.167. The distribution width parameters w_2 and w_3 accordingly increase.

The crystals of the third component become donors of mass with increasing treatment time because after 73 h, their fraction decreases by a factor of two to 0.011, and the average size decreases. As a result, some crystals of the third component complement the crystal fractions of the second and first components.

The first component is the main donor of the transferred mass: although A_1 slightly increases between 45 and 73 h of treatment, the average size and hence the mass of the particles of this component drastically decrease. This indicates that the structure of its crystals is most mobile. The mobility of the crystal structure was explained [1, 26, 28, 29] by the multitude of cleavage–formation acts of Me–O bonds and the accompanying defect formation under the conditions of quasi-equilibrium of the reversible hydroxylation of oxide in the aqueous fluid. The structure disordering facilitates the mobility, but the appearance of mobility leads to structure ordering, which was observed many times for simple and complex oxides formed at the dehydroxylation stage [29–36].

The process is most conspicuous in the case of the transformation of amorphous silica into quartz [32, 34, 37, 38]. At first, at 400°C and a water fluid pressure of 20–30 MPa, hydroxylation of silica leads to structure disordering with bound water content increasing by a factor of 3–15 (up to 3.8% [40]) depending on the state of silica [32, 39]. The structure mobility increases, reaching its maximum in the quasi-equilibrium state. Then the structure ordering causes dehydroxylation, forming intermediate phases and ends with formation of the quartz structure [29, 32, 37, 38]. The dehydroxylation rate drastically decreases, but the process continues for a long time, while the quartz structure is improved in the supercritical water fluid, and the contents of residual hydroxyl groups decrease 3.3-fold from 1000 to 300 ppm [37].

Thus, the differences in the mobility of corundum crystals structure for different components of the size spectrum and their role in mass transfer may be caused by differences in the hydroxylation levels and the rates of structure ordering. While the crystal formation mechanisms of the second and fourth components are similar, the tendencies in the variation of the distribution parameters (Table 1) during recrystallization differ. At the start of the process, the crystals of the second component along the radial thickness wholly consist of the overgrown layer; the average size m_2 is almost constant, but the amount of substance in this component (A_2) and the distribution width (w_2 parameter) constantly increase. The overgrown layer of the crystals of the fourth component covers the hydroxyl-free grain of electrocorundum; at the same time, both the fraction of the particles of this component (A_4) and their size (m_4 and w_4 parameters) change insignificantly during the process. Accordingly, the properties of the corundum layer overgrown under similar external conditions in different components are not identical.

Regarding the crystal structure mobility in an aqueous fluid, this effect evidently underlies the new methods for the preparation of oxide ceramics: cold sintering process (CSP) [41, 42]; hydrothermal sintering [43] or reactive hydrothermal liquid-phase densification (rHLPD) [44, 45]; and water-assisted flash sintering (WAFS) [46]. In all instances when high-density ceramics was obtained, the aqueous medium plays the key role in the transition from conventional molding at high temperatures to molding between room temperature and 300°C. This effect is similar to the object of investigation in the present study with a characteristic transition from the temperature of 1000–1200°C required for the preparation of α-Al_2O_3 from hydrargillite in air or vacuum to the temperature of 400°C sufficient for the transformation in and aqueous medium [1, 26].

CONCLUSIONS

The lognormal function may be used because both nucleation and further crystal growth occur under the influence of various factors on a random variable (crystal size) with already accumulated effects of previous treatments; i.e., the process occurs in a system with multiplicative properties. A detailed procedure was formulated for the use of the lognormal function for processing the electron microscopy data and determining the particle size distribution with a justified choice of the number of components. When the physical meaning of one of the distribution parameters (dispersion) was interpreted, which affects the distribution asymmetry, it was concluded that the parameter is related to the nonuniformity of crystal formation conditions.

An analysis of the change in the particle size of finely crystalline corundum kept for a period of time from 21 to 73 h at 400°C and a supercritical fluid pressure of 26.7 MPa showed that after the corundum formation was completed, the mass transfer continues and recrystallization of the finely crystalline powder occurs. The size spectrum of microcrystals in the lognormal distribution format has four components, each of which has characteristics with a clear physical meaning: A_i is the coefficient proportional to the number of crystals, m_i is the average crystal size, and w_i is the width (form) of the distribution function (which is determined by the nonuniformity of crystal formation conditions). The appearance of several components of crystal distribution during the formation of corundum is determined by the different routes of crystal formation in the nonuniform reaction space. Two spatially separated components (the second and fourth ones) form due to the collective absorption of nuclei; the first and third components form due to spontaneous coalescence of the remaining nuclei in the space around the crystals of the second and fourth components, respectively. The distribution components are preserved during recrystallization. However, the characteristics of the lognormal distribution function of the components A_i, m_i, and w_i change. An analysis of the changes allows us to reveal the

difference between the properties of the crystals of different components and trace their evolution.

Based on the character of the changes in the average crystal size and the fractions of components, it was concluded that the crystal structures of different components have different mobilities and that corundum in crystals of free generation is not identical to corundum that covers the corundum grain of the initiating additive.

REFERENCES

1. Yu. D. Ivakin, M. N. Danchevskaya, and G. P. Muravieva, Russ. J. Phys. Chem. B **9**, 1082 (2015).
2. G. M. Zimina, V. I. Zolotarevskii, D. V. Krasnyi, and A. A. Revina, High Energy Chem. **38**, 226 (2004).
3. N. W. Jenkins, S. B. Mirov, and V. V. Fedorov, J. Lumin. **91**, 147 (2000).
4. H.-B. Fan, S.-Y. Yang, P.-F. Zhang, H.-Y. Wei, X.-L. Liu, C.-M. Jiao, Q. S. Zhu, Y.-H. Chen, and Z.-G. Wang, Chin. Phys. Lett. **24**, 2108 (2007).
5. R. Sánchez Zeferino, M. Barboza Flores, and U. J. Pal, Appl. Phys. **109**, 014308 (2011).
6. M. A. AL-Jalali, I. F. Aljghami, and Y. M. Mahzia, Int. J. Chem. Tech. Res. **8**, 116 (2015).
7. L. Lin, J. Liu, J. Lv, S. Shen, X. Wu, D. Wu, Y. Qu, W. Zheng, and F. Lai, J. Alloys Compod. **695**, 1523 (2017).
8. H. L. Green and W. R. Lane, *Particulate Clouds: Dusts, Smoke, and Mists. Their Physics and Physical Chemistry and Industrial and Environmental Aspects* (Khimiya, Moscow, 1972; Van Nostrand, Princeton, NJ, 1964).
9. N. N. Gavrilova, V. V. Nazarov, and O. V. Yarovaya, *Microscopic Methods for Determining the Particle Size of Dispersed Materials* (RKhTU im. D. I. Mendeleeva, Moscow, 2012) [in Russian].
10. E. Limpert, W. A. Stahel, and M. Abbt, BioScience **51**, 341 (2001).
11. T. Grönholm and A. Annila, Math. Biosci. **210**, 659 (2007).
12. H. Mouri, Phys. Rev. E **88**, 042124 (2013). doi 10.1103/PhysRevE.88.042124
13. E. Limpert and W. A. Stahel, PLoS One **6**, e21403 (2011). doi 10.1371/journal.pone.0021403
14. V. E. Gmurman, *Probability Theory and Mathematical Statistics* (Vysshaya shkola, Moscow, 1972) [in Russian].
15. O. G. Raabe, J. Aerosol Sci. **2**, 289 (1971).
16. A. N. Kolmogorov, Dokl. Akad. Nauk SSSR **31**, 99 (1941).
17. R. Bergmann and A. Bill, J. Cryst. Growth **310**, 3135 (2008).
18. K. S. Lokovic, R. B. Bergmann, and A. Bill, Mater. Res. Soc. Symp. Proc. **1245**, A16-07 (2010).
19. A. Bill and R. B. Bergmann, in *Proceedings of the Symposium DD – Artificially Induced Crystalline Alignment in Thin Films and Nanostructures, 2011,* Vol. 1308, mrsf10-1308-dd03-01. https://doi.org/10.1557/ opl.2011.506
20. A. P. Kalinin, V. V. Manoilov, and O. A. Prikhod'ko, Nauch. Priborostr. **24** (4), 38 (2014).
21. J. Heintzenberg, Aerosol Sci. Technol. **21**, 46 (1994).
22. V. Tomashevskii and E. Zhdanova, *Simulation in the GPSS Environment* (Bestseller, Moscow, 2003) [in Russian].
23. S. Banerjee, B. Menkiel, and L. C. Ganippa, Appl. Phys. B **96**, 571 (2009).
24. M. A. Stetsenko, Optoelektron. Poluprovodn. Tekh., No. 49, 93 (2014).
25. C. M. Tan, N. Raghavan, Thin Solid Films **516**, 8804 (2008).
26. Yu. D. Ivakin, M. N. Danchevskaya, O. G. Ovchinnikova, G. P. Murav'eva, and V. A. Kreisberg, Sverkhkrit. Fluidy Teor. Prakt. **3** (4), 11 (2008).
27. A. A. Aleksandrov and B. A. Grigor'ev, *Tables of Thermophysical Properties of Water and Water Vapor, Reference Book* (Mosk. Energet. Inst., Moscow, 1999) [in Russian].
28. Yu. D. Ivakin, A. I. Zui, T. P. Murav'eva, and M. N. Danchevskaya, Vestn. Mosk. Univ., Ser. Khim. **42**, 258 (2001).
29. Yu. D. Ivakin, G. P. Murav'eva, S. N. Torbin, and M. N. Danchevskaya, Vestn. Mosk. Univ., Ser. Khim. **38**, 312 (1997).
30. Yu. D. Ivakin, M. N. Danchevskaya, P. A. Yanechko, and G. P. Murav'eva, Vestn. Mosk. Univ., Ser. Khim. **41**, 89 (2000).
31. A. V. Maryashkin, Yu. D. Ivakin, M. N. Danchevskaya, G. P. Murav'eva, and M. N. Kirikova, Mosc. Univ. Chem. Bull. **66**, 290 (2011).
32. M. N. Danchevskaya, G. P. Panasyuk, and V. B. Lazarev, Zh. Vseross. Khim. Ob-va im. Mendeleeva **36**, 706 (1991).
33. M. N. Danchevskaya, Yu. D. Ivakin, S. N. Torbin, G. P. Panasyuk, V. N. Belan, and I. L. Voroshilov, High Press. Res. **20**, 229 (2001).
34. M. M. Danchevskaya, Yu. D. Ivakin, G. P. Muravieva, and I. V. Luchkov, J. Phys.: Conf. Ser. **121**, 082001 (2008). http://iopscience.iop.Org/article/10.1088/1742-6596/121/8/082001/pdf.
35. Yu. D. Ivakin, M. N. Danchevskaya, and G. P. Muravieva, High Press. Res. **20**, 87 (2001).
36. M. N. Danchevskaya, Yu. D. Ivakin, S. N. Torbin, G. P. Muravieva, and O. G. Ovchinnikova, J. Mater. Sci. **41**, 1385 (2006).
37. M. N. Danchevskaya, Yu. D. Ivakin, S. N. Torbin, and G. P. Muravieva, J. Supercrit. Fluids **42**, 419 (2007).
38. M. N. Danchevskaya, S. N. Torbin, G. P. Muravieva, O. G. Ovchinnikova, and Yu. D. Ivakin, Reactiv. Solids **5**, 293 (1988).
39. M. N. Danchevskaya, V. A. Kreisberg, and V. N. Rakcheev, Zh. Fiz. Khim. **62**, 122 (1988).
40. M. N. Danchevskaya, O. G. Ovchinnikova, V. A. Kreisberg, and V. N. Rakcheev, Zh. Fiz. Khim. **62**, 1867 (1988).
41. J.-P. Maria, X. Kang, R. D. Floyd, E. C. Dickey, H. Guo, J. Guo, A. Baker, S. Funihashi, and C. A. Randall, J. Mater. Res. **32**, 3250 (2017).
42. J. Gonzalez-Julian, K. Neuhaus, M. Bernemann, J. Pereira da Silva, A. Laptev, M. Bram, and O. Guillon, Acta Mater. **144**, 116 (2018).
43. H. Guo, J. Guo, A. Baker, and C. A. Randall, ACS Appl. Mater. Interfaces **8**, 20909 (2016).
44. K. Yanagisawa, M. Nishioka, K. Ioku, and N. Yamasaki, J. Mater. Sci. Lett. **12**, 1073 (1993).
45. A. Ndayishimiye, A. Largeteau, M. Prakasam, S. Pechev, M.-A. Dourges, and G. Goglio, Scr. Mater. **145**, 118 (2018).
46. J. Nie, Y. Zhang, J. M. Chan, R. Huang, and J. Luo, Scr. Mater. **142**, 79 (2018).

Translated by L. Smolina